DOI 10.1007/s10946-016-9561-0
Journal of Russian Laser Research, Volume 37, Number 2, March, 2016

INFLUENCE OF ELEMENTAL COMPOSITIONS IN LASER CLEANING FOR AUTOMOTIVE COATING SYSTEMS

Mohammad Khairul Azhar Abdul Razab,[1]* Mohamad Suhaimi Jaafar,[2] Nor Hakimin Abdullah,[1] Mohamad Faiz Mohd Amin,[1] and Mazlan Mohamed[1]

[1] *Advanced Material Research Cluster, Faculty of Earth Science Universiti Malaysia Kelantan Jeli Campus Locked Bag No. 100, 17600 Jeli, Kelantan, Malaysia*

[2] *School of Physics, Universiti Sains Malaysia Main Campus 11800 Minden, Penang, Malaysia*

*Corresponding author e-mail: azhar@umk.edu.my

Abstract

Laser coating removal is an approach that has the potential to replace conventional chemical-based stripping methods in industry. In addition to the laser parameters, the efficiency of this cleaning technique depends also on the coating system itself. For this reason, we study the influence of the elemental compositions of two Malaysian automotive coated substrates, referred to here as A and B, on laser coating removal mechanisms using the Cynosure Cynergy Nd:YAG laser. The optimum laser coating removal efficiencies for both samples A and B are determined based on the depths of 360 craters obtained using a given formula. Selected crater depths on both of the stipulated samples are then subjected to energy dispersive X-ray analysis to determine their elemental compositions. The results indicate that sample A, which has higher aluminum content, shows greater efficiency in coating system removal, with balanced carbon and oxygen compositions aiding coating reduction during the cleaning process.

Keywords: laser cleaning, Nd:YAG laser, energy dispersive X-ray analysis, coating systems.

1. Introduction

Theoretically, laser cleaning can be distinguished in terms of two subareas: the removal of unwanted installed layers and the removal of unwanted contamination layers from solid surfaces [1]. Both areas include the cleaning of foreign organic impurities from metal substrates and the removal of existing coatings from metal surfaces [2, 3]. Previous studies have indicated that laser cleaning procedures for coating removal have tremendous potential to replace conventional chemical wet cleaning methods, which consume large amounts of water and are costly [4–6].

Laser cleaning methods also have the advantages of causing no mechanical damage to the metal surface while simultaneously increasing the effectiveness of the coating removal process [7]. The unique characteristics of laser cleaning provide a versatile, precise, controllable, selective, and environmentally-friendly process to strip unwanted coatings from substrate surfaces in industry [8, 9].

Laser coating removal involves a few complex mechanisms, including photothermal, photochemical, and mechanical effects, in which the exact mechanisms depend on the laser parameters and the physical

Manuscript submitted by the authors in English first on February 1, 2016 and in final form on March 31, 2016.

and chemical properties of the coating material [10]. The coating removal mechanism begins after the absorption of the laser intensity in the coating layers has exceeded the ablation threshold of the material [6, 8–12]. In general, the average coating removal efficiency depends on the elemental composition of the coated material itself, along with the suitability of the laser parameters that have been used [4, 13].

Current research indicates that laser cleaning offers a good alternative to replace conventional chemical cleaning methods in coating removal applications in various industries, including the automotive industry [9,11–15]. However, information on the ways in which the elemental compositions of automotive coating systems will influence the removal efficiency is not well documented because of a lack of research studies on the subject in this industry. This paper will therefore provide some empirical data obtained from energy dispersive X-ray (EDX) analysis performed on laser irradiated and nonirradiated cleaning procedures conducted on coated substrates from the Malaysian automotive industry. The study aims to investigate the relationships and effects of coating elemental compositions in an automotive laser coating removal system.

2. Laser Coating Removal

Thirty-six rectangular coated car substrate samples were acquired from two Malaysian national car models, designated A and B, with metallic acrylic coating systems that have never been repainted. Each substrate sample of types A and B was marked using unique numbers from 1 to 18 and was subjected to 10 laser irradiations using a Nd:YAG laser, as shown in Fig. 1. The laser fluence F was increased by 10 J/cm^2 for each shot, and the pulse width (PW), repetition rate (RR), and beam size (BS) were all manipulated as listed in Table 1. Thus, a total of 360 irradiations was performed for all substrate samples of types A and B.

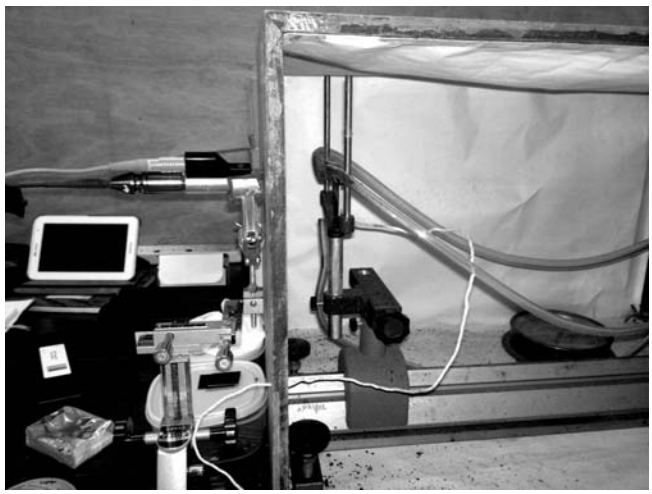

Fig. 1. Experimental set-up used for laser coating removal from Malaysian coated automotive substrates.

The originality of the structure, the pattern, the contour, and the texture of the irradiated crater depth were determined along with any physical and chemical distortion sustained before proceeding to the energy dispersive X-ray (EDX) analysis.

We determine the average coating removal efficiency for each of the irradiated samples using the following equation [16, 17]:

$$\epsilon = V/E = d/nF, \tag{1}$$

where ϵ is the average coating removal efficiency in $\mu\text{m} \cdot \text{cm}^2 \cdot \text{J}^{-1}$, V and d are the volume and depth of coating removed, while E, F, and n are the total laser energy, laser fluence, and number of laser shots, respectively.

The removal depths d are shown with respect to the incident laser fluence F for each pulse width, repetition rate, and beam size. Therefore, ϵ for each set of laser parameters when applied to a specific sample is determined by measuring the inclination slope of each fitted linear graph.

Table 1. Variations in Laser Parameters: Laser Fluence, Pulse Width, Repetition Rate, and Beam Size.[a]

Sample number	Number of irradiations	Beam size, BS mm	Laser fluence, F J/cm^2	Pulse width, RW ms	Repetition rate, RR Hz
1	10	3	210–300	100	1.0
2	10	3	210–300	200	1.0
3	10	3	210–300	300	1.0
4	10	3	210–300	100	1.5
5	10	3	210–300	200	1.5
6	10	3	210–300	300	1.5
7	10	3	210–300	100	2.0
8	10	3	210–300	200	2.0
9	10	3	210–300	300	2.0
10	10	5	150–240	100	1.0
11	10	5	150–240	200	1.0
12	10	5	150–240	300	1.0
13	10	5	150–240	100	1.5
14	10	5	150–240	200	1.5
15	10	5	150–240	300	1.5
16	10	5	60–150	100	2.0
17	10	5	60–150	200	2.0
18	10	5	60–150	300	2.0

[a]Maximum laser fluence for the 3-mm beam is 300 J/cm^2 for all laser parameters, whereas maximum laser fluence for the 5 mm beam is 240 J/cm^2 for repetition rates of 1.0 and 1.5 Hz, and 150 J/cm^2 for a repetition rate of 2.0 Hz.

Table 2. Optimum Crater Depths Selected from the Highest and Lowest ϵ of Substrate Samples A and B.

Substrate sample	Selected substrate sample	Selected crater depth	Criterion
A	A 10	No. 7	Optimum of sample A
	Nonirradiated sample A	Random	Control of sample A
B	B 11	No. 3	Optimum of sample B
	Nonirradiated sample B	Random	Control of sample B

In this study, we measured d for each crater depth of samples A and B using the Alicona infinite focus metrology (IFM) G4 (Alicona Imaging GmbH, Graz, Austria). We investigated the elemental compositions based on a selected crater depth from selected substrate samples with higher and lower ϵ, as shown in Table 2. Selection of the optimum crater depths for samples A and B is based on compensation of the best evaluations of the Alicona IFM G4 optical images with the naked eye and acceptable ranges of lower surface roughness results, as shown in Fig. 2. In addition, a nonirradiated area

was selected randomly from each of the two types of nonselected substrate samples to act as a control for this analysis.

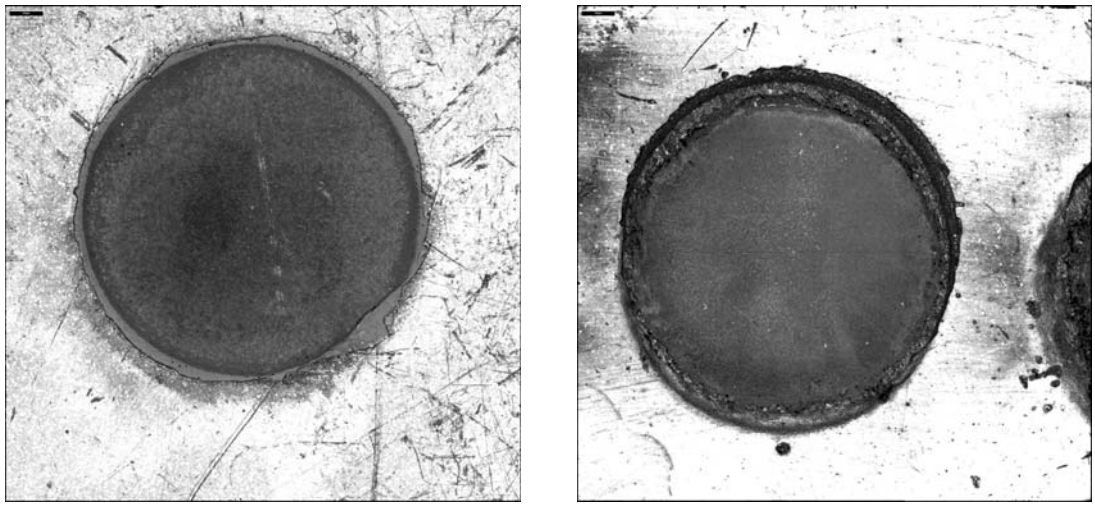

Fig. 2. Infinite focus metrology (IFM) image (a) for pulse width of 100 ms, repetition rate of 1.0 Hz, beam size of 5 mm, and laser fluence of 180 J/cm^2 for sample A10 at crater depth No. 7 with 5× magnification, and IFM image (b) for pulse width of 200 ms, repetition rate of 1.0 Hz, beam size of 5 mm and laser fluence of 220 J/cm^2 for sample B11 at crater depth No. 3 with 5× magnification.

3. Energy Dispersive X-Ray Analysis

Energy dispersive X-ray (EDX) analysis provides the percentages of the atomic numbers of atoms (at.%) and the percentages of the atomic weights (wt.%) of each of the identified elements. The EDX is an analytic system integrated into the Nova NanoSEM 450 scanning electron microscope system; additional hardware such as the X-Max50 silicon drift detector and the PentaFET precision spectroscopic detector are included, along with the Advanced Aztec Synergy package software (Oxford Instruments, Abingdon, UK) for EDX data collection and processing at the selected crater depth, as shown in Fig. 3.

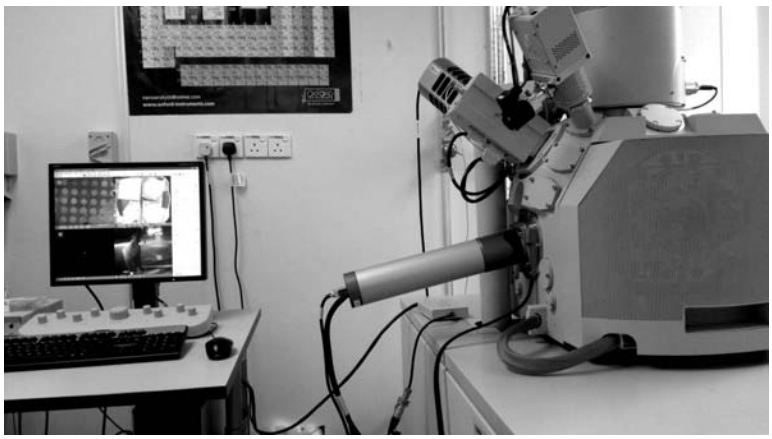

Fig. 3. Nova NanoSEM 450 with integrated EDX system to perform elemental composition analysis on the targeted region of interest. Here, computer unit used for image morphology and EDX analysis (a) and NanoSEM 450 chamber (b).

The initial EDX analysis process usually involves generation of an X-ray spectrum from the entire region of interest (ROI) scanned by the field emission scanning electron microscopy (FESEM). The backscattered electron (BE) image in the scanning electron micrograph displays the elemental compositional contrast acquired from the different atomic numbers of the elements and their distributions. The elemental compositions for each selected crater depth were presented in an X/Y graph form. The Y axis shows the counts (i.e., the number of X-rays received and processed by the detector), while the X axis shows the energy levels of those counts. The Advanced Aztec Synergy package software was used to determine the energy levels of the K-shell X-rays of specific elements to obtain the elemental compositions.

For this analysis, the electron beam was kept stationary on a targeted spot at a selected crater depth to generate X-ray spectra, which then provided localization of the elemental information. A line was drawn on the scanning electron micrograph to generate a plot of the relative proportions of the previously identified elements along the spatial gradients. Finally, the distributions and relative proportions of the previously defined elements were mapped over the scanned area for elemental population identification.

4. Elemental Composition Characteristics at Each Selected Crater Depth

4.1. Sample A

In Fig. 4, we show the peaks of the elemental compositions that were obtained from sample A10 at crater depth No. 7. These results represent the optimum selected crater depth for sample A. In addition, the peaks of the elemental compositions for the nonirradiated top coating surface layer of sample A were also analyzed, and the results are shown in Fig. 5.

The elemental compositions that were detected by the EDX analytic system for all selected crater depths of sample type A are listed in Tables 3 and 4 in terms of percentages of the atomic numbers of the atoms (at.%) and percentages of their atomic weights (wt.%). From these results, 10 elements were detected for sample A10 at crater depth No. 7, as shown in Table 3. In contrast, only four elements were detected for the nonirradiated sample A, as shown in Table 4.

Table 3. Composition Arranged by Percentage of Atomic Number of Atoms (at.%), Percentage of Atomic Weight (wt.%), and Percentage of Sigma Weight (wt. sigma %) of Each Element Identified Using a Pulse Width of 100 ms, a Repetition Rate of 1.0 Hz, a Beam Size of 5 mm and Laser Fluence of 180 J/cm^2 for Sample A10.

Element	at.%	wt.%	wt. sigma %
C	33.65	17.78	1.34
O	37.13	26.12	1.51
Na	2.05	2.08	0.58
Mg	0.62	0.66	0.2
Al	2.52	2.99	0.31
Si	2.61	3.23	0.33
P	6.87	9.36	0.68
Ti	3.84	8.08	0.95
Ni	3.63	9.36	4.38
Zn	7.08	20.34	1.36
Total:	100	100	–

4.2. Sample B

In Fig. 6, we show the peaks of the elemental compositions for sample B11 at crater depth No. 3. The selected crater depth was considered to be the optimum depth for sample B.

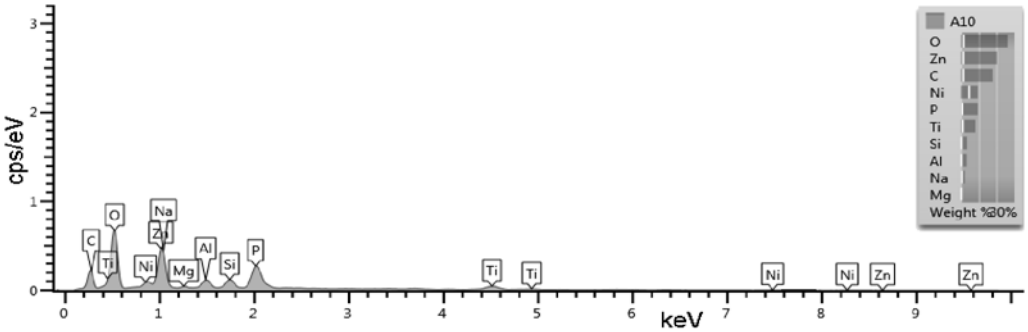

Fig. 4. Elemental compositions for pulse width of 100 ms, repetition rate of 1.0 Hz, beam size of 5 mm, and laser fluence of 180 J/cm^2 for sample A10. Ten elements were detected on the ROI selected at 10 kV using the EDX system, including Mg, Na, and Ni.

Fig. 5. Elemental compositions for nonirradiated sample A. Four elements were detected on the ROI selected at 10 kV using the EDX system and included C, O, N, and Ti.

Fig. 6. Elemental compositions for pulse width of 200 ms, repetition rate of 1.0 Hz, beam size of 5 mm, and laser fluence of 220 J/cm^2 for sample B11. Nine elements were detected on the ROI selected at 10 kV using the EDX system, including Na, Al, and Ti.

Fig. 7. Elemental composition of nonirradiated sample B. Four elements were detected on the region of interest selected at 10 kV using the energy dispersive X-ray system, including C, O, Si, and Ti.

Table 4. Composition Arranged by Percentage of Atomic Number of Atoms (at.%), Percentage of Atomic Weight (wt.%), and Percentage of sigma Weight (wt. sigma %) of Each Element Identified in Nonirradiated Sample A.

Element	at.%	wt.%	wt. sigma %
C	65.63	58.22	2.41
N	14.4	14.9	3.08
O	18.57	21.95	1.45
Ti	1.4	4.94	0.91
Total:	100	100	–

Table 5. Composition Arranged by Percentage of Atomic Number of Atoms (at.%), Percentage of Atomic Weight (wt.%), and Percentage of sigma Weight (wt. sigma %) of Each Element Identified Using Pulse Width of 200 ms, Repetition Rate of 1.0 Hz, Beam Size of 5 mm, and Laser Fluence of 220 J/cm^2 for sample B11.

Element	at.%	wt.%	wt. sigma %
C	44.62	25.66	0.96
O	32.76	25.09	0.83
Na	1.41	1.55	0.41
Al	0.34	0.45	0.16
Si	0.82	1.11	0.18
P	6.39	9.48	0.46
Ti	5.42	12.43	0.8
Fe	3.31	8.85	1.62
Zn	4.92	15.4	0.75
Total:	100	100	–

Table 6. Composition by Percentage of Atomic Number of Atoms (at.%), Percentage of Atomic Weight (wt.%), and Percentage of sigma Weight (wt. sigma %) of Each Element Identified in Nonirradiated Sample B.

Element	at.%	wt.%	wt. sigma %
C	80.55	73.69	0.84
O	18.11	22.06	0.75
Si	0.45	0.96	0.17
Ti	0.9	3.28	0.56
Total:	100	100	–

In addition, in Fig. 7 we show the peaks of the elemental compositions for a nonirradiated sample B.

Tables 5 and 6 list the elemental compositions for all selected crater depths of sample B in terms of percentage of atomic number of atoms (at.%) and percentage of atomic weight (wt.%). Nine elements were detected in sample B11, as shown in Table 5. In contrast, four elements were detected in the nonirradiated sample B, as shown in Table 6.

5. Influence of Elemental Compositions on Coating Removal Efficiency

The EDX results show that all of the irradiated selected samples A and B demonstrated pre-treatment coatings nearest to the bare metal. This was proven by detection of elemental Zn, which was recognized as the main component of an anticorrosive coating and simultaneously acted to enhance the adhesion between the coating and the metal substrate, as shown in Tables 3 and 5 [18]. Other nonmetallic elements such as oxygen (O) and carbon (C), which changed their atomic weights during the stripping process, were also detected. The decreasing C numbers and increasing numbers of O elements on irradiated samples A

and B have shown that some parts of the plasma cleaning process occur via oxidation processes [18].

The laser coating removal mechanisms for all irradiated samples were considered not to have reached the bare metal, in that the detected O composition was still increasing. It was found that oxygen composition monitoring had given full indications of bare metal surface generation. This is because of the removal of the primer and pre-treatment coatings, which will reduce the oxygen composition to a minimum level when the bare metal surface was reached [19].

In addition, the results also showed that the number of elemental compositions that was detected using EDX increased with increasing crater depth, as demonstrated by the results in Table 3 for sample A and Table 5 for sample B. The analysis found that C and O elements predominantly existed on the top coatings of the two substrate samples, whereas some of the other elemental compositions were only traced as the crater depth developed [18]. Tracing of the chemical compositions depends on the crater depth, texture, and structure that were obtained along with the elemental compositions of the painted material itself, where the interior layers of the coating system were exposed.

The arrangement of the elemental compositions in sample A is the more effective of the two for laser coating removal mechanisms, where the reduction of the atomic percentages of its C (33.65%) and O (37.13%) element levels are uniform after laser irradiation. This indicated that laser cleaning mechanisms consisting of photothermal and photoablation processes occurred actively in this type of coating system [14]. This may be attributed to the thermal distribution, which was uniform on the crater surface of sample A but was randomly distributed on sample B. One contributing factor may be that the coating material in sample B has the lowest diffusivity and is thus unable to distribute the laser thermal energy effectively. This condition results in a nonuniform distribution of the "thermal pool," which leads to reduced effectiveness for the thermal decomposition process in the coating material [20].

The average coating removal efficiency ϵ also highly depends on the percentage of aluminum flakes embedded in the base coat of the coating system. Aluminum flakes enhance the thermal distribution because of their high thermal conductivity [20]. The results show that sample A contained a higher aluminum percentage of 2.52% when compared with that of sample B, which has only 0.34%, as shown in Tables 3 and 5, respectively.

The laser absorption ability also depends on the carbon particle content of the coating material, which is highly absorptive at the 1.06-μm laser wavelength. However, the balancing effect of elemental O was also influential in terms of surface oxidation for the coating removal process. The percentages of C and O in the coating system are the main factors that affect the efficiency of the laser removal mechanism.

In this case, the nonirradiated sample A has a better balance of C (65.63%) and O (18.57%) element contents when compared with that of the nonirradiated sample B, which has an imbalanced C (80.55%) and O (18.11%) content, as shown in Tables 4 and 6, respectively. Balancing of the elemental C and O compositions inside the surface coating layers triggered the absorption of the laser beam for the rapid coating removal process, whereby the re-solidification caused by carbonization processes at the surface was reduced [18, 21–23]. Therefore, the threshold fluence for sample B was much higher than that for sample A because of the re-solidification due to carbonization processes, which had been increasing at the irradiated surface [6].

6. Conclusions

Laser cleaning techniques offer numerous advantages for use in the automotive industry, particularly, for use in coating removal systems that do not affect the mechanical and physical properties of the bare

metal underneath. In the technique proposed, the elemental compositions of the automotive coating systems are shown to have a major influence on the effectiveness of the removal process based on the balancing of C and O contents during photothermal and photoablation removal processes. In this study, we also found that automotive coating systems with higher percentage contents of aluminum flakes are more efficient when using laser coating removal mechanisms.

Acknowledgments

We acknowledge the support of the Short Term Research Grant Scheme awarded by Universiti Malaysia Kelantan under Grant No. R/SGJP/A08.00/00451A/001/2015/000241. We express our appreciation to Mr. Yahya Ibrahim and Mrs. Ee Bee Choo of the School of Physics, Universiti Sains Malaysia, and Mr. Ahmad Fadli Ahmad Sanusi of the Faculty of Earth Science, Universiti Malaysia Kelantan Jeli Campus for their help in preparation of the laser equipment and its accessories during the experiments and the EDX analysis. Our grateful thanks also go to Miss Illya Syazwanie Ahmad Mazalan of the Faculty of Earth Science for acting as a data accumulator for this research project.

References

1. D. Bäuerle, *Laser Processing and Chemistry*, 4th ed., Springer, Berlin (2011).
2. D. M. Kane, *Laser Cleaning*, World Scientific, Singapore (2006), Vol. II.
3. J. P. Nilaya and D. Biswas, *Pramana J. Phys.*, **75**, 1087 (2010).
4. W. M. Steen and J. Mazumder, *Laser Material Processing*, 4th ed., Springer, Berlin (2010).
5. A. Kumar, R. Bhatt, P. Behere, et al., *Pramana J. Phys.*, **82**, 237 (2014).
6. M. K. A. A. Razab, M. S. Jaafar, A. A. Rahman, and S. A. Saidi, *Appl. Mech. Mater.*, **554**, 439 (2014).
7. V. Veiko, T. J. Mutin, V. Smirnov, et al., "Fundamentals of laser assisted micro- and nanotechnologies," *Proc. SPIE*, **6985**, 69850D (2008).
8. J. Lee and K. Watkins, *Opt. Lasers Eng.*, **34**, 429 (2000).
9. Y. K. Madhukar, S. Mullick, S. S. Chakraborty, and A. K. Nath, *Procedia Eng.*, **64**, 467 (2013).
10. Y. S. Koh, "Laser cleaning as a conservation technique for corroded metal artifacts," Ph.D. Thesis, Luleå University of Technology, Sweden (2006).
11. G. Chen, T. Kwee, K. Tan, et al., *Appl. Phys. A*, **101**, 249 (2010).
12. Y. K. Madhukar, S. Mullick, and A. K. Nath, *Appl. Surf. Sci.*, **286**, 192 (2013).
13. T. Naguy and R. Straw, Report "Laser technology for aerospace maintenance and sustainment applications," Air Force Research Laboratory, Wright-Patterson Air Force Base, Ohio, USA (2010).
14. M. K. A. A. Razab, M. S. Jaafar, A. A. Rahman, et al., "Influence of threshold fluence, absorption coefficient and thermal loading in laser paint removal mechanisms," in: *Environment, Energy, and Applied Technology*, CRC Press (2015), p. 885.
15. M. K. A. A. Razab, M. S. Jaafar, A. A. Rahman, and S. Affandi Saidi, *Adv. Environ. Biol.*, **8**, 227 (2014).
16. D. Roberts, *Appl. Phys. A*, **79**, 1067 (2004).
17. X. Zhou, K. Imasaki, H. Furukawa, et al., *Surf. Coatings Technol.*, **137**, 170 (2001).
18. C. Cottam, D. Emmony, A. Cuesta, and R. Bradley, *J. Mater. Sci.*, **33**, 3245 (1998).

19. E. B. Siggs, "Laser and electron beam treatments for corrosion protection of friction stir welds in aerospace alloys," Ph.D. Thesis, University of Birmingham, UK (2010).
20. M. K. A. A. Razab, M. S. Jaafar, and A. A. Rahman, *Int. J. Eng. Technol.*, **14**, 39 (2014).
21. J. Arthur, R. Bowman, and R. Straw, Final Technical Report "Robotic laser coating removal system," in *Environmental Security Technology Certification Program*, Arlington, Virginia, USA (2008).
22. S. Georgiou, "Laser cleaning methodologies of polymer substrates," in: K. L. Thomas (Ed.), *Polymers and Light*, Springer, Berlin (2004), p. 1.
23. L. Li, W. M. Steen, P. J. Modern, and J. T. Spencer, *Proc. SPIE*, **2246**, 84 (1994).